

Visualization of Fast Ion Phase-Space Flow Driven by Alfvén Instabilities

journal or publication title	Physical Review Letters
volume	127
number	23
page range	235002
year	2021-12-01
NAIS	13264
URL	http://hdl.handle.net/10655/00013373

doi: <https://doi.org/10.1103/PhysRevLett.127.235002>



Visualization of Fast Ion Phase-space Flow Driven by Alfvén Instabilities

X.D. Du,¹ M.A. Van Zeeland,¹ W.W. Heidbrink,² J. Gonzalez-Martin,² K. Särkimäki,³ A. Snicker,⁴ D. Lin,² C.S. Collins,¹ M.E. Austin,⁵ G.R. McKee,⁶ Z. Yan,⁶ Y. Todo,⁷ and W. Wu¹

¹General Atomics, P.O. Box 85608, San Diego, California 92186-5608, USA

²University of California, Irvine, California 92697, USA

³Department of Physics, Chalmers University of Technology, SE-41296 Göteborg, Sweden

⁴Department of Applied Physics, Aalto University, P.O. Box 11100, 00076 AALTO, Finland

⁵University of Texas-Austin, Austin, Texas 78712, USA

⁶University of Wisconsin-Madison, Madison, Wisconsin 53706-1687, USA

⁷National Institute for Fusion Science, 509-5292 Toki, Japan

(Dated: October 28, 2021)

Fast ion phase-space flow, driven by Alfvén eigenmodes (AEs), is measured by an imaging neutral particle analyzer in the DIII-D tokamak. The flow firstly appears near the minimum safety factor at the injection energy of neutral beams, and then moves radially inward and outward by gaining and losing energy, respectively. The flow trajectories in phase space align well with the intersection lines of the constant magnetic moment surfaces and constant $E - (\omega/n)P_\zeta$ surfaces, where E , P_ζ are energy and toroidal canonical momentum of ions; ω and n are angular frequencies and toroidal mode numbers of AEs. It is found that the flow is so destructive that the thermalization of fast ions is no longer observed in regions of strong interaction. The measured phase-space flow is consistent with nonlinear hybrid kinetic-magnetohydrodynamics simulation. Calculations of the relatively narrow phase-space islands reveal that fast ions must transition between different flow trajectories to experience large-scale phase-space transport.

PACS numbers:

1 Wave-particle interaction is a universal phenomenon 30
 2 of great importance in physical systems, including as- 31
 3 trophysics, laser physics, and many others. In magnet- 32
 4 ically confined fusion devices, wave-particle resonances 33
 5 can drive massive fast-ion transport across phase space. 34
 6 Predicting and minimizing this transport is a key issue 35
 7 to achieve a sustainable burning plasma in fusion reac- 36
 8 tors. Past studies measure fast ion profiles, averaging 37
 9 over a broad portion of phase space, to study global 38
 10 confinement [1–7]. However, wave-particle interactions 39
 11 occur locally in phase space and resonant fast ions mi- 40
 12 grate along certain phase-space routes, something which 41
 13 has not been measured before. Understanding the phase- 42
 14 space flow formation and its evolution are important is- 43
 15 sues that could impact operation of nuclear fusion reac- 44
 16 tors. It is fundamental to the development of predictive
 17 modeling, control techniques to mitigate fast ion loss and
 18 advanced operation scenarios, such as utilizing the alpha
 19 channelling effect [8]. Transport by Alfvén eigenmodes
 20 (AE) is a particular concern. To address this, an imaging
 21 neutral particle analyzer (INPA) [9, 10] was developed in
 22 the DIII-D tokamak. The first ever visualization of fast
 23 ion phase space flow driven by AEs is reported here.

24 The INPA measures energetic neutrals, which are pro-
 25 duced by charge-exchange reactions between confined
 26 fast ions and an active neutral beam source, as seen from
 27 Fig. 1(a). The system covers nearly all radii, and resolves
 28 the neutral energies from ~ 30 keV to ~ 100 keV. The
 29 diagnostic sensitivity or ‘weights’ of $\sim 1\%$ of the available

INPA pixels in the radius-energy plane, depicted as the
 white circles in Fig. 1(b), are estimated using the syn-
 thetic diagnostic code (INPASIM) [11, 12]. Each circle
 corresponds to the contour lines of 30% of the maximum
 weights. The INPASIM also finds that fast ions with the
 pitch v_{\parallel}/v from ~ 0.77 to 0.84 can be collected by INPA,
 illustrated as the black band (v_{\parallel} refers to the fast ion ve-
 locity parallel to the magnetic field line). Note that the
 validation of the INPA system [9, 10] and synthetic mod-
 eling [11] in a broad range of plasma parameters were
 systematically reported in [11, 13].

The orbit topology over the INPA-interrogated phase
 space, computed by the orbit tracing code (ASCOT5)
 [14], is overlaid. The system interrogates the phase space
 occupied by well-confined fast ions on stagnation orbits

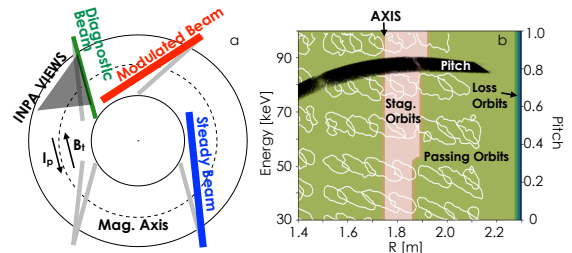


FIG. 1: (a) the neutral beam geometry, along with the INPA view. (b) the weight function of the INPA (circles) on energy-radius plane, along with the measured pitch range. The orbit topology in the INPA-interrogated phase space is overlaid.

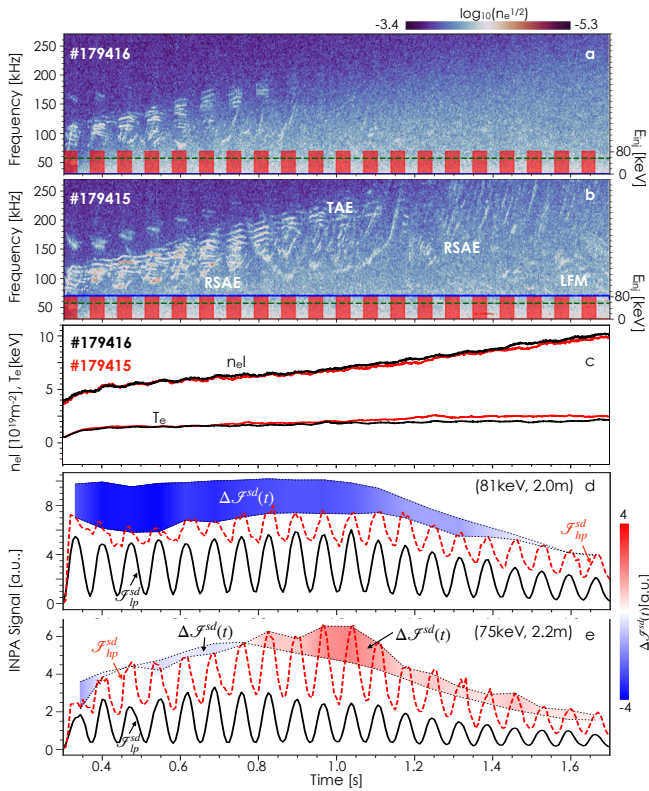


FIG. 2: Frequency spectra of the density fluctuation for the low-power shot (a) and high-power shot (b), along with the waveforms of the neutral beams. (c) The time evolution of line-integrated n_e and T_e . The measured INPA signal in the low-power shot (solid line) and high-power shot (dashed line) and the signal deficit to the expectation of the neoclassical theory (colormap) for the velocity space ($E \sim 81$ keV, $R \sim 2.0$ m) (d) and ($E \sim 70$ keV, $R \sim 2.2$ m) (e).

near the magnetic axis and on passing orbits elsewhere. Stagnation orbits are a class of orbits which are confined on a given side of the magnetic axis near the device mid-plane which travel in a single toroidal direction. The view does not cover the confined-loss boundary.

A controlled experiment is designed to visualize the phase-space flow in the plasma current ramp-up phase, at a toroidal magnetic field of ~ 2.1 T and in an upper single null magnetic configuration. The strategy is to vary AE activities in a pair of shots as much as possible, with a minimum change of the plasma parameters and equilibrium. As seen from Fig. 2(a), the plasma with less or no AE activity in the low-power (lp) shot (#179416) is heated by two neutral beams, i.e., a steady diagnostic neutral beam at 55 keV of 1 MW and a modulated beam at 81 keV of 2.5 MW with a cycle time of 70 ms and a duty cycle of 50%. The INPA detects the charge-exchanged neutral flux from a time-evolving slowing-down (sd) fast ion distribution. That is, the image above 55 keV can be expressed as $\mathcal{I}_{lp} \equiv \mathcal{I}_{lp}^{sd}(t)$.

The AE activity in Fig. 2(b) are largely enhanced af-

ter adding a steady (st) beam of ~ 82 keV at a modest beam power of ~ 1.7 MW. The beam is injected at the axisymmetry angle of the modulated beam. Thus, the image in the high-power (hp) shot can be expressed as, $\mathcal{I}_{hp} \equiv \mathcal{I}_{hp}^{sd}(t) + \mathcal{I}_{hp}^{st}$, where \mathcal{I}_{hp}^{st} is the image produced by the steady beam.

As seen from Fig. 2(c), the electron density n_e agrees well in the pair of shots, due to a delicate tuning of the n_e feedback control system. The electron temperature T_e also agrees well before ~ 1.0 s, and starts to deviate later. In this circumstance, neoclassical theory expects $\mathcal{I}_{lp}^{sd}(t) = \mathcal{I}_{hp}^{sd}(t)$. This is experimentally demonstrated by a quantitative agreement of $\mathcal{I}_{lp}^{sd}(t)$ and $\mathcal{I}_{hp}^{sd}(t)$, when AEs are stable, and further supported by the agreement with synthetic INPA images, using the fast ion distribution predicted by NUBEAM module of TRANSP [15]. For details, see the Supplemental Material [16].

As expected, when AEs are unstable, $\mathcal{I}_{lp}^{sd}(t)$ and $\mathcal{I}_{hp}^{sd}(t)$ deviate. Figures 3 and 4 compare images at two different modulation periods in these two discharges. In Fig. 3 at ~ 1.0 s, the AE activity is absent in low-power shot and relatively weak in high-power shot (see Fig. 3(a4) and (b4)); while in Fig. 4 at ~ 0.38 s, the AE activity appears even in low-power shot and is quite strong in high-power shot (see Fig. 4(a4) and (b4)). In both cases, three snapshots at three different times in the beam modulation cycle are shown to illustrate the birth and subsequent slowing-down of ions from the modulated source. Even when the AE activity is relatively weak, noticeable differences between images in the two shots appear (Fig. 3). Although the n_e profiles match, less full-energy fast ions appear in the plasma core in the high-power shot. Moreover, in spite of a slightly higher edge T_e by $\sim 10\%$ in the high-power shot, more INPA signal appears at the reduced energy of ~ 75 keV at $R > 2.1$ m, as indicated by the arrows. These features are in contrast to expectations from neoclassical theory, which would predict: (i) for the same density profile, the ionization profile of fast ions is expected to be the same; (ii) for a higher edge T_e , the slowing-down time is longer and thus less INPA signal at the lower energy range is expected for the high power shot. For convenience, the red (blue) colored region in Fig. 3(c1)-(c3) are called an inflow (outflow) region, where the amount of the confined fast ions are above (below) that in the low-power shot.

The deviation of $\mathcal{I}_{lp}^{sd}(t)$ and $\mathcal{I}_{hp}^{sd}(t)$ is even more significant, when the AE activity is strong (Fig. 4). The differences are: (i) The INPA signal of the modulated beam at the injection energy of 82 keV, indicated by the dotted lines, is mostly missing in the high-power shot, as seen from Figs. 4(b1)-(b3). It suggests a full depletion of ionized neutrals in a time scale much shorter than the camera integration time of 0.5 ms. That is, when AEs are unstable even in the low-power shot (see Fig. 4(a4)), the phase space in high-power shot exhibits strong self-organized criticality dynamics. (ii) The slowing-down of

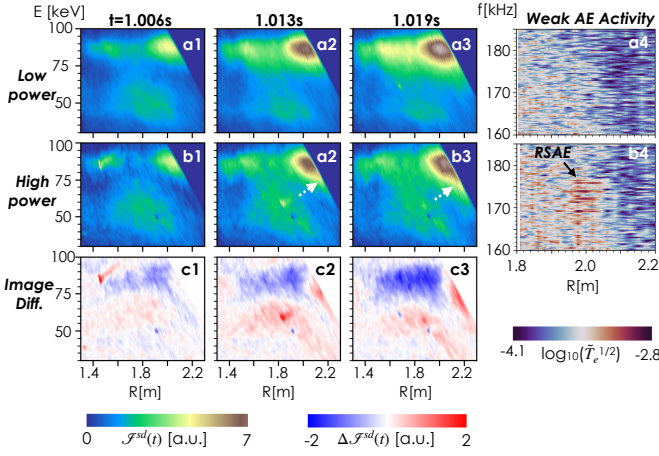


FIG. 3: INPA images of the modulated beam source during the weak AE activity (from 1.006s to 1.019s). (a1)-(a3) Low power shot 179416. (b1)-(b3) High power shot 179415. (c1)-(c3) Difference image. T_e fluctuation in low-power shot (a4) and in high-power shot (b4) at ~ 1.013 s.

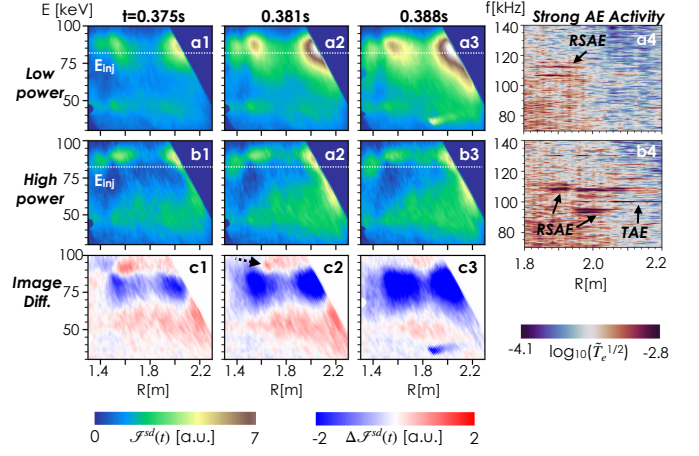


FIG. 4: INPA images of the modulated beam source during strong AE activity (from 0.375s to 0.388s). (a1)-(a3) Low power shot 179416. (b1)-(b3) High power shot 179415. (c1)-(c3) Image difference. T_e fluctuation in low-power shot (a4) and high-power shot (b4) at ~ 0.381 s.

1 fast ions is not observed across the image series in the
 2 high-power shot, which is consistent with the fact that
 3 the increase of T_e is barely noticeable in the plasma core
 4 after adding neutral beam power of 1.7 MW (see Fig. 5
 5 2(c)). (iii) As seen from the highlighted image differ-
 6 6 ences $\Delta\mathcal{I}^{\text{sd}}(t) \equiv \mathcal{I}_{\text{hp}}^{\text{sd}}(t) - \mathcal{I}_{\text{lp}}^{\text{sd}}(t)$ in Fig. 4(c1)-(c3), an
 7 inflow region (red) in the plasma core emerges, as indi-
 8 8 cated by the arrow. It shows radially inward transport
 9 of fast ions with energies exceeding the injection energy
 10 of 82 keV. It should be mentioned that the image pat-
 11 11 tern of the $\Delta\mathcal{I}^{\text{sd}}(t)$ smoothly evolves, as AEs activities
 12 are gradually diminishing from 0.3 s to 1.7 s.

13 These changes in $\Delta\mathcal{I}^{\text{sd}}(t)$ depend on the strength of
 14 the AE activity. Figures 2(d) and 2(e) show the time
 15 evolution of the flows for two INPA pixels. For a pixel
 16 near the radius of the strongest AE activity ($R = 2.0$ m)
 17 near the injection energy of ~ 81 keV, strong outflow is
 18 observed that steadily decreases as the AE activity weak-
 19 19 ens in time (see Fig. 2(d)). For a pixel at lower energy
 20 and larger radius, inflow occurs for intermediate levels
 21 of AE activity, then ceases when the AEs become stable
 22 (see Fig. 2(e)). No inflow is observed during the early
 23 phase of very strong AE activity at the end of modulation
 24 periods. During this phase, the strong edge toroidicity-
 25 induced AE (TAE) activity (see Fig. 4(b4)) prevents re-
 26 26 distribution of fast ions in the outer region of $R > 2.1$ m
 27 at reduced energy of $E < 75$ keV.

28 To understand the connection of the observed inflow
 29 (red) and outflow (blue) areas across the phase space,
 30 fast ion migration trajectories are reconstructed, referred
 31 to as the streamlines below. It is known that the mag-
 32 32 netic moment μ is conserved during resonant interactions
 33 with AEs as long as the AE frequency is much lower than
 34 the ion cyclotron frequency. Moreover, $E' \equiv E - \omega P_{\zeta}/n$
 35 is also conserved [7], where P_{ζ} is the toroidal canoni-

cal momentum; ω and n are the angular frequency and
 toroidal mode number of the AE, respectively. To si-
 multaneously satisfy the constraints, the streamline must
 follow the intersection of the curved, constant μ and E'
 planes in phase space. The curved μ and E' planes in
 the coordinate $(E, R, v_{\parallel}/v)$ are calculated by ASCOT5
 and the intersection of two planes, i.e., E' & μ stream-
 lines, is identified. Owing to the finite pitch (v_{\parallel}/v) re-
 solution discussed in Fig. 1(b), a majority part of the
 E' & μ streamlines may intersect the phase space volume
 interrogated by the INPA. By scanning μ and E' , and
 all observed ω/n , we reconstruct the streamlines in the
 INPA views, given as the dotted lines in Fig. 5(a). The
 streamline, associated with dominant reversed-shear AE
 (RSAE), having $n = 2$, $l = 0$, $f = 86$ kHz in plasma
 frame, is labeled as b1; the streamlines of RSAE with
 $n = 2$, $l = 1$ and $f = 89$ kHz for two E' constants are
 given as b2 and b3. (l : the number of nodes in the radial
 eigenmode envelope). Note that these streamlines are
 most relevant to the observed image pattern, since they
 pass through the radial positions of the minimum safety
 factor q_{min} at $R \sim 2.0$ m near the beam injection en-
 ergy, and connect the outflow region and two inflow re-
 gions together. Besides, the majority part of streamlines,
 related to edge TAEs with lower ω/n , does not intersect
 the INPA-interrogated phase space and only a small portion
 appears well below the injection energy.

The phase-space flow is further investigated, using
 a nonlinear, kinetic-magnetohydrodynamics (MHD) hy-
 36 36 brid code (MEGA) [17–19]. The simulation uses the mea-
 37 37 sured plasma profiles, the equilibrium reconstructed by
 38 38 EFIT [20] and fast ion distributions (\mathcal{F}_{fi}) from NUBEAM
 39 39 module of TRANSP [15] at ~ 0.44 s as the initial condi-
 40 40 tions. The \mathcal{F}_{fi} evolves in three separated periods in the

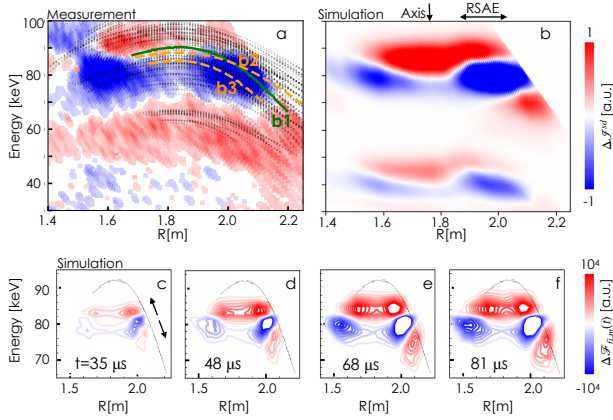


FIG. 5: (a) The measured flow images in (a), along with the streamlines; (b) the simulated flow image using MEGA-estimated fast ion distributions at INPA measured pitch of ~ 0.78 ; time evolution of the fast ion distributions in (c)-(f) by MEGA simulation.

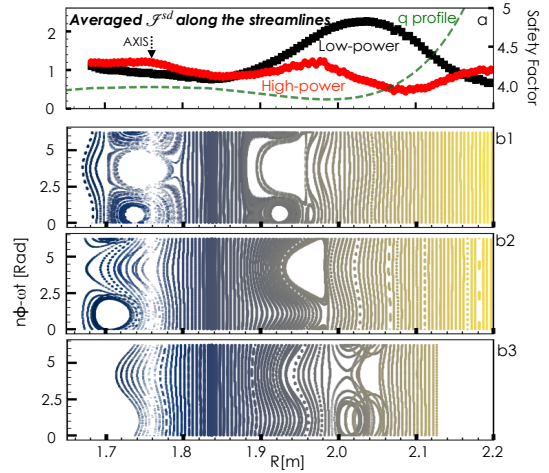


FIG. 6: (a) The averaged INPA signal along the streamlines b1-b3 in Fig. 5 in the LP shot (black) and in the HP shot (red), along with the q profile. The estimated phase-space islands along these streamlines b1-b3 in (b1)-(b3), respectively.

1 absence of MHD instabilities. This is to simulate the fast
 2 ion thermalization process. Following each period, the
 3 kinetic-MHD hybrid phases are conducted subsequently
 4 for 0.1 ms and the RSAEs of $n=2$ are routinely identi-
 5 fied. Meanwhile, the $\mathcal{F}_{fi,m}$, i.e., the fast ion distribution
 6 related to the modulated beam, is largely modified at
 7 INPA interrogated pitch of 0.78. As one example, fig-
 8 ures 5(c)-(f) present the change of $\mathcal{F}_{fi,m}$ at 35, 48 and
 9 81 μs after RSAE excitation in the third hybrid phase.
 10 It is found that the outflow (blue) and the inflow (red)
 11 region expands along the streamline, revealing formation
 12 of RSAE-driven, fast ion phase space flow. Here, the
 13 streamline b1, indicated by the black curve, is overlaid
 14 as the reference. The synthetic INPA image in Fig 5(b)
 15 is obtained by a convolution integral of the $\mathcal{F}_{fi,m}$ at 81 μs
 16 and the computed weight function. The result reproduces
 17 the observed inflow (red) and outflow (blue) regions in
 18 phase space, showing a reasonable agreement with the
 19 averaged $\Delta\mathcal{I}^{\text{sd}}$ images in Fig. 5(a). It is worth pointing
 20 out that the further expansion of the outflow (blue) re-
 21 gion towards the boundary of INPA view (see Fig 4(c3)),
 22 caused by the edge TAE modes, has not been reproduced
 23 by MEGA. The discrepancy below 60 keV is also specu-
 24 lated to be due to the lack of the TAE modes, which will
 25 be addressed in future work.

26 AEs flatten the fast ion-density along E' & μ stream-
 27 lines. The $\mathcal{I}_p^{\text{sd}}$, averaged over the labeled streamlines in
 28 Fig. 5(a), shows a hollow profile with a peak near the
 29 q_{min} location at $R = 2.0$ m in the low-power shot, as
 30 seen from the black line in Fig. 6(a). This is because
 31 the neutral beam nearly tangential to the magnetic field
 32 line populates the magnetic axis region with a pitch of
 33 ~ 0.68 , outside of the INPA-interrogated pitch [10]. In
 34 contrast, the $\mathcal{I}_p^{\text{sd}}$ in the high-power shot is significantly
 35 flattened along the streamline (red line in Fig. 6(a)).

36 To understand the transport mechanism, the phase-

space islands along the labeled streamlines b1-b3 in Fig.
 5(b) are studied using ASCOT5 code [14] and the re-
 sults are given in Figs. 6(b1) -(b3). These island chains
 are generated by the wave-particle resonant interactions
 and visualized by the Poincaré plots of fast ions orbits
 in presence of RSAE modes. Fast ions with constant
 $\mu = 18$ keV/T, interrogated by the INPA, are launched
 along the streamlines from the midplane. The radial
 structures of RSAE are obtained by a kinetic-MHD sta-
 bility analysis code (NOVA-K) [21] and selected accord-
 ingly, based on the T_e fluctuation measured by electron
 cyclotron emission (ECE) [22]. The amplitude of each
 AE is carefully calibrated using magnetic field line trac-
 ing technique, which is able to determine the magnetic
 perturbation from the measured \tilde{T}_e profiles by mapping
 constant T_e along magnetic field lines. Note that the
 transient maximum amplitude of AEs are used, instead
 of the averaged value from Fast Fourier transform.

As seen from Figs. 6(b1)-(b3), good Kolmogorov-
 Arnold-Moser surfaces widely exist along each stream-
 line. In other words, fast ions cannot flow freely along
 a single streamline to travel across the system. On
 the other hand, the observed flattening region is much
 broader than the widths of the phase-space islands.
 This contradiction suggests that fast ions cross between
 streamlines to achieve the large-scale phase space flow.
 One mechanism of streamline crossing is the natural in-
 tersection of streamlines with different values of ω/n . For
 example, the intersection of streamlines b1 and b2 would
 increase the phase-space flow traveling distance by 8 cm,
 as seen in Fig. 6(b1) and (b2); A second mechanism is
 scattering by collisions or turbulence from one streamline
 to a neighboring streamline of different radial extent. For
 example, the streamline b2 and b3 from the same RSAE
 are close to each other in Fig. 5(a). However, their phase

space islands drift by ~ 8 cm, as seen from Fig. 6(b2) and (b3). It is hypothesized that the intermittency of fast ion avalanche transport [23] may be due to the sudden increase of the streamline crossing, either by the transient excitation of new instabilities or the randomized turbulence.

In summary, the first ever visualization of fast ion phase space flow driven by AEs is reported here. It is found that the phase space flow is a ‘two-way traffic’ i.e., inward transport towards higher energy and outward transport to reduced energy, determined by relative velocity of fast ions and their initial positions to the waves during resonant interactions. The result is consistent with non-linear kinetic-MHD hybrid simulations. For the first time, flattening of the fast ion distribution function along E' & μ streamlines has been directly measured. When AEs are unstable even in the low-power shot, the phase space along the streamline shows strong self-organized criticality dynamics in high-power shot, i.e., an open system with a fast relaxation mediation by the threshold [24]. The transport along the streamline is compared to the widths of phase-space islands, generated by the resonant interactions with AEs. The result shows that streamline crossing, either due to the natural intersection of streamlines or small pitch-angle scattering by turbulence or collisions, plays a key role for the large-scale phase-space transport.

The author (X.D. Du) would like to thank M. Podestà, G.J. Kramer and R. Nazikian for fruitful discussions. This work was supported by the US DOE under DE-AC05-00OR22725, DE-FC02-04ER54698, DE-AC02-09CH11466, DE-SC0015878. The ASCOT5 project has received funding from the European Research Council under the European Union’s Horizon 2020 research and innovation program under grant agreement No 647121.

[1] W.W. Heidbrink and G.J., Sadler, Nucl. fusion 34, 535 (1994).
 [2] A. Fasoli, C. Goremnzano, H.L. Berk et al., Nucl. Fusion 47, S264 (2007).
 [3] B.N. Breizman and S.E. Sharapov, Plasma Phys. Controlled Fusion 53, 054001 (2011).
 [4] TOI, K., OGAWA, K., ISOBE, M., et al., K. Toi, K. Ogawa, M. Isobe et al., Plasma Phys. Controlled Fusion

53, 024008 (2011).
 [5] N.N. Gorelenkov, S.D. Pinches, K. Toi, Nucl. Fusion 54, 125001 (2014).
 [6] K. McClements and E.D. Fredrickson, Plasma Phys. Controlled Fusion 59, 053001 (2017).
 [7] Y. Todo, Reviews of Modern Plasma Physics (2019) 3:1 (2019).
 [8] N. J. Fisch, Phys. Rev. Lett. 41, p. 873 (1978)
 [9] X.D. Du, M.A. Van Zeeland, W.W. Heidbrink and D. Su, Nucl. Fusion 58, 082006 (2018).
 [10] M.A. Van Zeeland, X.D. Du, W.W. Heidbrink, L. Stagner, and D. Su, JINST 14, C09027 (2019).
 [11] X.D. Du, M.A. Van Zeeland, W.W. Heidbrink and L. Stagner and D. Su, Nucl. Fusion 60, 112001 (2020).
 [12] W.W. Heidbrink, D. Liu, Y. Luo, E. Ruskov and B. Geiger, Commun. Comput. Phys. 10 716 (2011).
 [13] D.J. Lin, X.D. Du, W.W. Heidbrink and M.A. Van Zeeland, Nucl. Fusion 60, 112008 (2020).
 [14] E. Hirvijoki, O. Asunta, T. Koskela, T. Kurki-Suonio, J. Miettunen, S. Sipila, A. Snicker, S. Akaslompolo Computer Physics Communications 185,1310–1321 (2014).
 [15] Pankin A., Mccune D., Andre R., Bateman G. and Kritiz A. Comput. Phys. Commun. 159 157 (2004).
 [16] See supplemental Material [url] for INPA images without AE activities, which includes references [11–13, 15, 25, 26].
 [17] Y. Todo and T. Sato., Phys. Plasmas 5, 1321–7 (1998).
 [18] Y. Todo, H. Berk and B. Breizman Nucl. Fusion 50, 084016 (2010).
 [19] Y. Todo, R. Seki, D.A. Spong, H. Wang, Y. Suzuki, S. Yamamoto, N. Nakajima and M. Osakabe, Phys. Plasmas 24, 081203 (2017)
 [20] L. Lao, H. St John, R. Stambaugh, A. Kellman and W. Pfeiffer, Nucl. Fusion 25, 1611(1985).
 [21] C. Z. Cheng, Phys. Rep. 1, 211 (1992).
 [22] M.A. Van Zeeland, G.J. Kramer, M.E Austin, R.L Boivin, W.W. Heidbrink, M.A. Makowski, G.R. McKee, R. Nazikian, W.M. Solomon, G. Wang, Phys. Rev. Lett. 97, 135001 (2006).
 [23] C.S. Collins, W.W. Heidbrink, M.E. Austin, G.J. Kramer, D.C. Pace, C.C. Petty, L. Stagner, M.A. Van Zeeland, R.B. White, Y.B. Zhu, Phys. Rev. Lett. 116, 095001 (2016).
 [24] R. Sanchez and D.E. Newman, Plasma Phys. Control. Fusion 57, 123002 (2015).
 [25] W.W. Heidbrink, M.A. Van Zeeland, M.E. Austin, A. Bierwage, Liu Chen, G.J. Choi, P. Lauber, Z. Lin, G.R. McKee and D.A. Spong, Nucl. Fusion 61, 016029 (2021)
 [26] G.J. Choi, P. Liu, X.S. Wei, J.H. Nicolau, G. Dong, W.L. Zhang, Z. Lin, W.W. Heidbrink and T.S. Hahm, Nucl. Fusion 61, 066007 (2021).